ARCHIVES
o f
FOUNDRY ENGINEERING

Morphology and Distribution of α-Al and Mn-rich Phases in Al-Si-Mn Alloys under an Electromagnetic Stirring

P. Mikolajczak (ID)
Poznan University of Technology, Poland
Corresponding author. E-mail address: Piotr.Mikolajczak@put.poznan.pl

Abstract

Convection caused by gravity and forced flow are present during casting. The effect of forced convection generated by a rotating magnetic field on the microstructure and precipitating phases in eutectic and hypoeutectic AlSiMn alloys was studied in solidification by a low cooling rate and low temperature gradient. The chemical composition of alloys was selected to allow joint growth or independent growth of occurring α-Al, α-Al$_{15}$Si$_2$Mn$_4$ phases and Al-Si eutectics. Electromagnetic stirring caused instead of equiaxed dendrites mainly rosettes, changed the AlSi eutectic spacing, decreased the specific surface S$_v$ and increased secondary dendrite arm spacing λ$_2$ of α-Al, and modified the solidification time. Forced flow caused complex modification of pre-eutectic and inter-eutectic Mn-phases (Al$_{15}$Si$_2$Mn$_4$) depending on the alloy composition. By high Mn content, in eutectic and hypoeutectic alloys, stirring caused reduction in the number density and a decrease in the overall dimension of pre-eutectic Mn-phases. Also across cylindrical sample, specific location of occurring phases by stirring was observed. No separation effect of Mn-phases by melt flow was observed. The study provided an understanding of the forced convection effect on individual precipitates and gave insight of what modifications can occur in the microstructure of castings made of technical alloys with complex composition.

Keywords: Casting microstructure, Aluminum alloys, Electromagnetic stirring, Solidification, Manganese phases

1. Introduction

Casting alloys based on aluminum are frequently used to produce simple and advanced engineering parts [1], e.g. in the automotive and in the aerospace industries. Main alloying elements in casting alloys are Cu, Si, and Mg, whilst the main impurities are iron (Fe), manganese (Mn) and zinc (Zn) in recycled alloys. Iron is the most harmful element causing formation of long intercepting platelets leading to unacceptable mechanical properties, thus alloying elements such as Be, Mo, Cr and especially Mn have been used to replace needle shaped β-Al$_5$FeSi phases with α-Al(Mn,Fe)Si skeleton or granular (or Chinese) morphology [1-3].

Started together with studies by Flemings on non-dendritic structures [4] with special rheological properties [5] developments allows: casting production with higher mechanical properties [6], semisolid metal processing (SSM) [7], by magnetohydrodynamics (MHD) [8] and by high shear melt conditioning (HSMC) [9]. In a technology called electromagnetic stirring (EMS) [10], flow of liquid driven by rotating magnetic fields (RMF) modify the alloys microstructure [11] and increases the properties.

Presence of manganese (Mn) in Al-Si alloys and the development of technologies using forced flow for melt conditioning needs more knowledge about occurring physical processes and microstructure modification during processing and in processed castings.

In this study in the spotlight were: the Al-Si-Mn system (ternary phase diagram on Figure 1), in terms of the phases like α-Al, α-Al$_{15}$Si$_2$Mn$_4$, the transformation of the whole microstructure and the modification in morphology of phases present that might be affected through artificial flow. The convection effect was studied in case of small cylindrically shaped casting samples. To know what is the effect on each of the phases, such composition was chosen, where only studied precipitate nucleate and grow (independent growth) from liquidus to solidus temperature. To know what may be effect of common growth (joint growth) of studied phases, also appropriate composition was selected.

Induced by forced convection, the whole microstructure and individual phases modification or separation was investigated, in aspect of the development in forced-flow technologies [5-11].

2. Materials and methods

From Al-Si-Mn phase diagram (Figure 1), the hypoeutectic and eutectic alloys were chosen and samples during solidification were processed without or with stirring generated by coils. In some defined alloys, only α-Al phase or only Mn-rich α-Al$_{15}$Si$_2$Mn$_4$ phases should grow from liquid melt. On the phase diagram, the solidification should follow exactly between monovariant lines, red, green or blue lines in Figure 1. In other defined alloys, common growth should occur, e.g. α-Al phase together with Mn-rich phases may grow. The remaining Al-Si eutectics and other phases should grow only at solidus temperature, so the solidification should follow one of the monovariant lines on phase diagram. Liquidus temperature 610 ˚C was chosen, and for some alloys 630 ˚C, by solidus temperature 575 ˚C. The alloys, where only one phase grow at beginning are:

- α-Al as first phase precipitates from the liquid alloy – the alloy labeled as "α-Al-first" (solid blue line on Figure 1), liquidus temperature T_L = 610 ˚C (AlSi7.887Mn0.379), and additionally, the alloy with T_L = 630 ˚C labeled as "α-Al-2-first" (AlSi4.896Mn0.254). Remaining phases (eutectics and manganese rich Al$_{15}$Si$_2$Mn$_4$) should only form at 575 ˚C,
- α-Al$_{15}$Si$_2$Mn$_4$ as first phase precipitates from the liquid alloy - the alloy labeled as "Mn-2-first" (solid red line on Figure 1), composition AlSi12.546Mn1.011, with T_L = 630 ˚C.

The alloys, where two phases simultaneously grow are:

- α-Al and Al$_{15}$Si$_2$Mn$_4$ start at 610 ˚C to grow together according to eutectic grove, marked with dashed violet line in Figure 1, composition AlSi7.798Mn0.835 - the alloy labeled as "α-Al/Mn", and eutectics may form at solidus temperature 575 ˚C,
- α-Al and Si crystals precipitate simultaneously - "α-Al/Si" alloy, composition AlSi12.536Mn0.296 (Figure 1, dashed yellow line), in this case was not possible to take T_L = 610 ˚C and the midpoint of the eutectic grove was chosen.

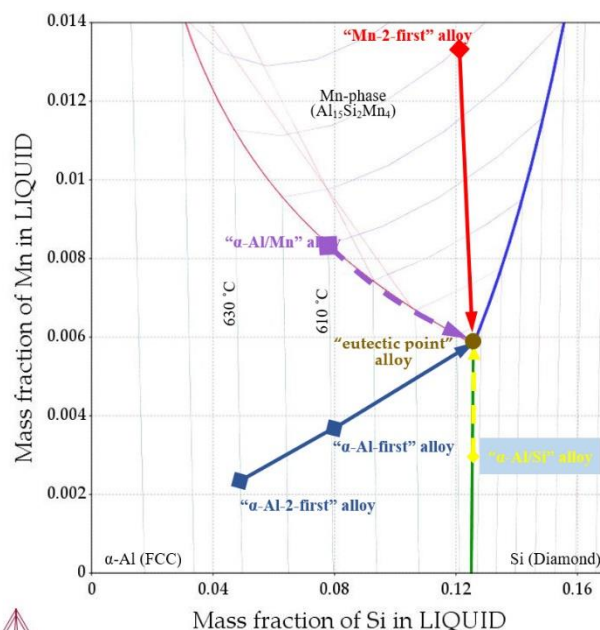The composition AlSi12.569Mn0.579 was selected for the sixth "eutectic point" alloy (Figure 1, brown point).

Fig. 1. Phase diagram of Al-Si-Mn system, with well visible paths for analyzed alloys, e.g. marked with dark blue line paths of α-Al-first (AlSi7.887Mn0.379) and α-Al-2-first (AlSi4.896Mn0.254) alloys. Paths determined according to method of Scheil–Gulliver calculation

An electric furnace was used for alloys melting (min. 1.5 h at 800–805 °C) from pure components: Mn (99.98% NewMet House, Essex, UK), Si (99.9999% NewMet House) and Al (99.999% HMW Hauner GmbH & Co. KG, Röttenbach, Germany), without any modifier, with argon degassing and flushing the crucible [12]. The cylindrical sample diameter of 38 mm was determined by graphite crucible, whilst the height of 65 mm in order to keep similar cooling conditions (solidification time). After 1.5 melting, the crucible filled with studied alloy was moved on the solidification position [12], where insulation (Fiberfrax, Unifrax, USA) allowed slow cooling and low temperature gradient, and electric coils were applied in order to generate melt flow during whole solidification. Temperature measurements [12-15] in the center and at the edge of sample and in the crucible, showed cooling rate $R_{800-liq}$ = 0.525 (K/s) and temperature gradient $G_{800-liq}$ = 0.194 (K/mm) without stirring.

The electric coils powered by autotransformer at frequency of 50Hz, voltage of 45V and electric current of 10A, generated rotating magnetic field (RMF) with 11 mT measured with Gaussmeter (MF100, Extech Instruments, US) [12].

The microstructure was studied on cross-section (Figure 2) cut out 10 mm from the cylindrical sample bottom. The specimens were grinded and polished using specialized facility Mecatech 250 SPC (Presi, Grenoble, France), whilst for observation of phases, LOM microscope (Nikon Eclipse MA200, Tokyo, Japan) was used. For determined 6 different alloys, 12 experiments were conducted, 6 without (0 mT) and 6 with stirring (11 mT). Based on the figures saved at different magnifications (from 50× to 500×) and by applied image stitching technique, e.g. secondary dendrite spacing, was measured in the ImageJ 1.51a software (National Institutes of

Health, USA). For the measurement and calculation of characteristic parameters, different areas (Figure 2) were selected: a) one general rectangle area (dashed blue line), b) four arch shaped areas (dotted blue line), c) four small rectangle shaped areas (white-filled).
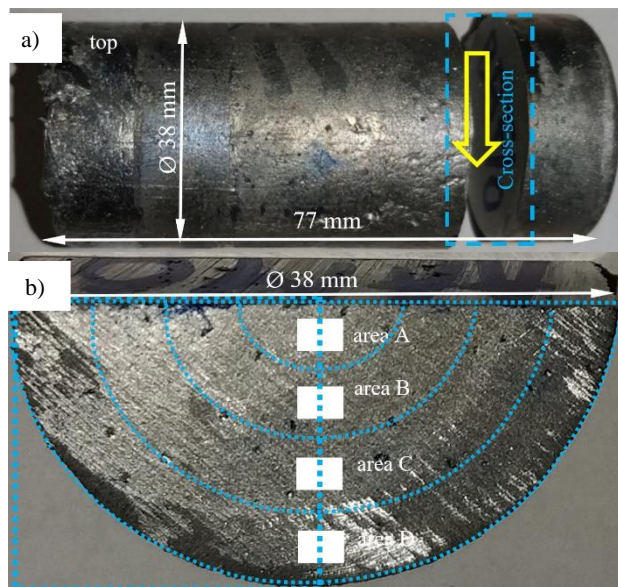

Fig. 2. Processed samples: a) place for the cross-section cutting out, b) arched and rectangular areas for parameters measurement. The blue dotted line shows arch shaped areas for the measurement of Mn pre-eutectic intermetallics and dendrite arm spacing (magnification 50×). The fulfilled white rectangles presents areas for e.g. eutectic spacing measurement (50× and 200×)

For the characterization of the flow effect on microstructure, following parameters were chosen and defined: average overall dimension L_{Mn} (Feret diameter) and number density n_{Mn} of α-$Al_{15}Si_2Mn_4$ precipitates, eutectic spacing λ_E for eutectics (by averaging distance between plates), secondary dendrite arm spacing λ_2 (by averaging distance between arms) and specific surface of dendrites S_v (measured from the enclosed area and the perimeter). 4697 of $Al_{15}Si_2Mn_4$ intermetallics were observed, and of this the overall dimension of 3075 inter-eutectic and 1622 pre-eutectic phases was measured and calculated. Averaging the distance between adjacent plates for spacing λ_E of AlSi eutectics was applied. The perimeter and the area of dendrites was used for determination of the specific surface of dendrites S_v. The well know secondary dendrite arm spacing λ_2 was based on 10-50 branches of dendrite.

The flow effect was studied in aspect of microstructure changes with occurring AlSi eutectics, dendritic or rosette shaped α-Al and complex shaped $Al_{15}Si_2Mn_4$ phases. These phases in aluminum alloys are known to author from earlier studies, projects and papers (e.g. in [1–3,14–19]). The composition of the proposed alloys was first determined based on available in the literature phase diagrams, but the exact composition and resulting precipitation sequence needed detailed calculations, in order to achieve the proposed, e.g. joint growth of two occurring phases beginning from liquidus till solidus temperature. Property diagrams, the precipitation sequence

and the Scheil solidification were analyzed in Thermo-Calc software [20].

3. Results

From experiments were collected microsections of the slowly solidified samples. For phases characterization, based on the measurement, the parameters were calculated and collected in tables. Also precise alloy compositions and precipitation sequences were calculated and presented in table and on figures.

3.1. Microstructure

Low cooling rate and low temperature gradient in the samples of α-Al-first alloy caused formation of α-Al equiaxed dendrites surrounded by Al-Si eutectics (Figure 3), during processing with natural only convection (0 mT). Induced by coils forced convection led to formation of α-Al shaped as rosettes and as spheroids (globular forms), but also some small dendritic α-Al occurred. Application of electromagnetic stirring for α-Al-2-first alloy, caused similar structure modification, but with less eutectics and more α-Al.
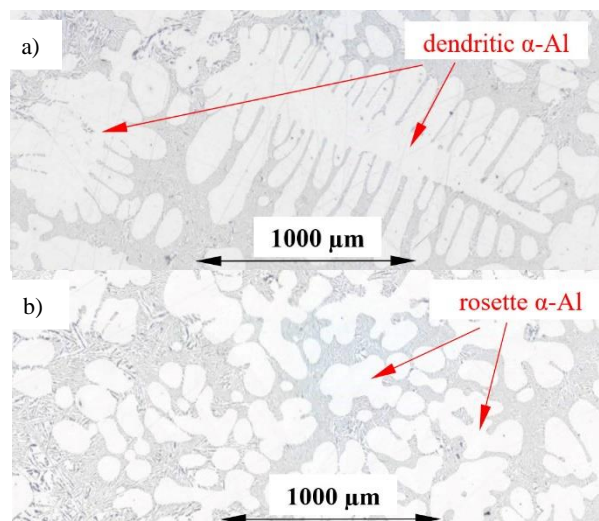

Fig. 3. Microstructures of the α-Al-first alloy processed by: (a) natural only convection (0 mT) and by (b) forced convection (11 mT). LOM, by 100× magnification

A microstructure of a Mn-2-first alloy, (Figure 4) where liquidus temperature reaches 630 ˚C, a high content of manganese caused formation of clearly visible shaped large and complex Mn-phases (Figure 5), precipitated similarly by natural only convection (Figure 4a, 5a) and by forced convection (Figure 4b, 5b) too. For solidification by natural convection (0 mT), the large phases (Figure 4a, 5a) may reach dimension of several millimeters but also much smaller precipitates occurred between Al-Si eutectics, whilst by melt flow (Figure 4b and 5b) the overall dimensions of $Al_{15}Si_2Mn_4$ phases seem to be smaller.

Fig. 4. Microstructures of the Mn-2-first alloy processed by: (a) natural only convection (0 mT) and by (b) forced convection (11 mT). LOM, by 25× magnification
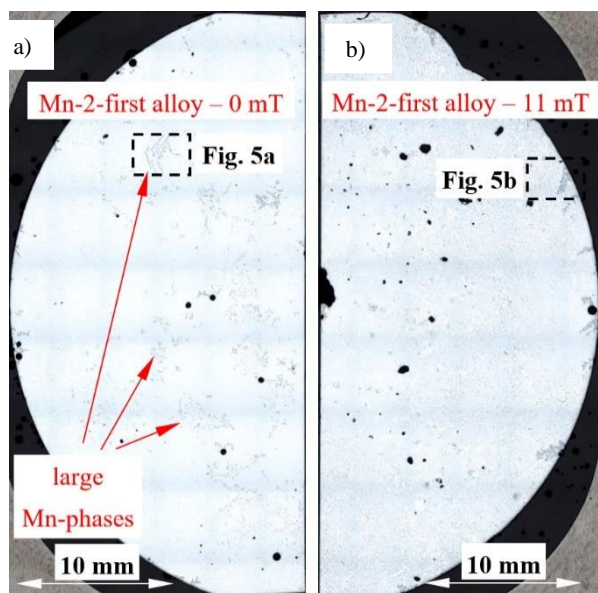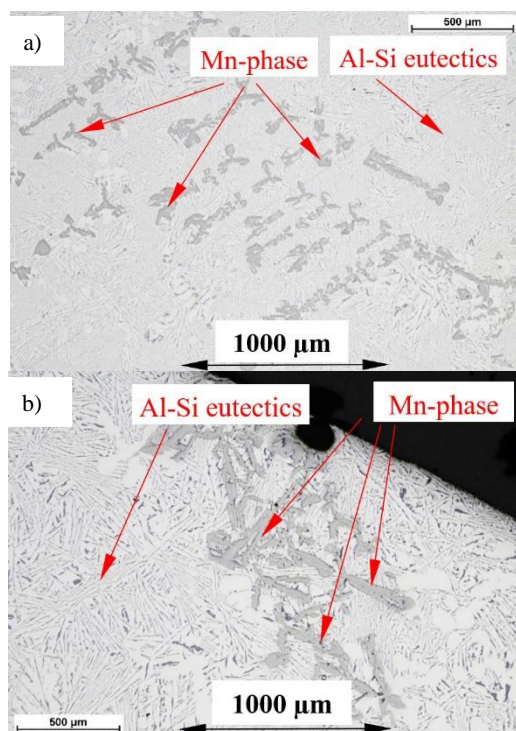

Fig. 5. Microstructures of the Mn-2-first alloy processed by: (a) natural only convection (0 mT) and by (b) forced convection (11 mT). LOM, by 100× magnification

For the AlSi7.798Mn0.835 alloy, labeled as α-Al/Mn, the structure across the samples solidified by natural only (Figure 6a) and by forced convection (Figure 6b), presents a homogenous distribution of $Al_{15}Si_2Mn_4$, eutectics and α-Al. For both

solidification conditions, Mn phases grew in the inter-dendritic cavities (Figure 7a) and formed according to the cavities shape, and otherwise freely shaped Mn-phases (Figure 7b) occurred.
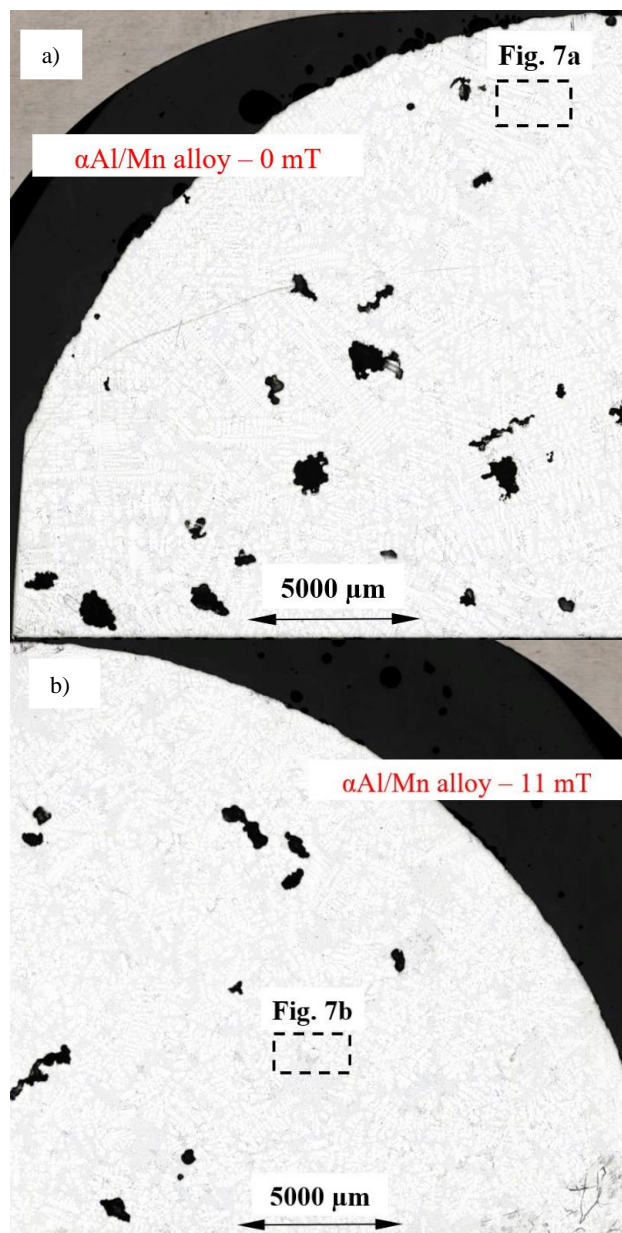

Fig. 6. Microstructures of the α-Al/Mn alloy processed by: (a) natural only convection (0 mT) and by (b) forced convection (11 mT). LOM, by 50× magnification

The Al-Si eutectics almost completely filled the structure (Figure 8) of the α-Al/Si alloy (AlSi12.536Mn0.296), with some $Al_{15}Si_2Mn_4$ and α-Al phases. Structure solidified without forced flow presented dendrites reaching the length up to 5 mm (Figure 8a), whilst by forced convection α-Al shaped as rosettes was significantly smaller (Figure 8b). Beside large dendrites and small rosettes, mainly an uniform distribution of phases was observed.
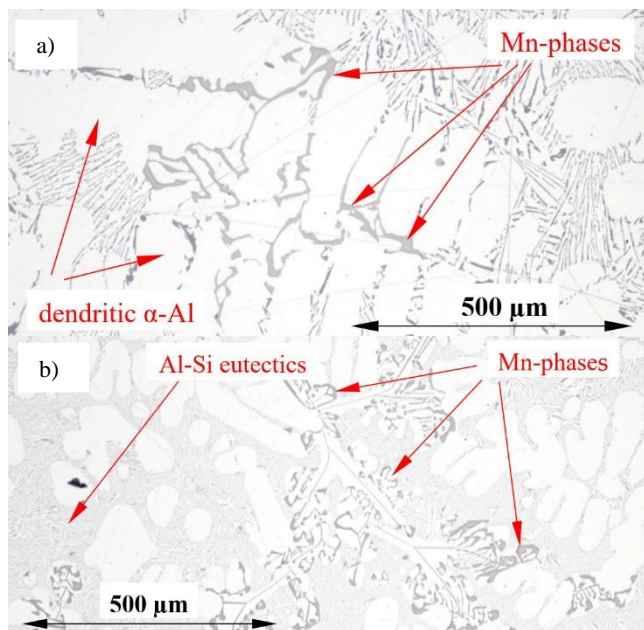
Fig. 7. Microstructures of the α-Al/Mn alloy specimen (a) with Mn-phases grown in inter-dendritic cavities (electromagnetic field 0 mT) and (b) with freely shaped Mn-phases (electromagnetic field 11 mT). LOM, by 200× magnification
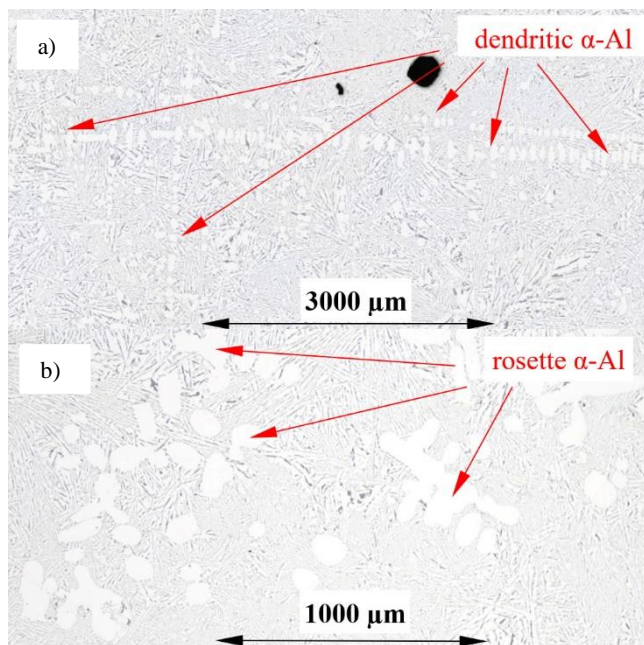

Fig. 8. Microstructures of the α-Al/Si alloy processed by: (a) natural convection (0 mT) and by (b) forced convection (11 mT). LOM, by 50× and 100× magnification

3.2. Parameters characterising microstructure

The influence of electromagnetically induced forced convection was described by help of several parameters determined on cut of samples (Figure 2). Applied methodology ensured trustworthy results collected in Tables 1-3 and presented a proper overview of all the specimens. For the high quality of the results, a lot of phases and crystals were measured and that allowed parameters calculation. The parentheses present number of inspected grains and counted arms, whilst square brackets presents standard deviation (Table 1-3). In the whole sample, on the selected 25 grains 248 arms were used to measure secondary dendrite arm spacing λ_2 that amounts 87 µm by calculated standard deviation of σ=5.9 µm. In comparison to natural only convection, forced convection increased dendrite spacing λ_2 by 9%. For natural only convection, the secondary dendrite arm spacing λ_2 amounts 86 µm (by standard deviation σ=3.3 µm), 104 µm (σ=5.2 µm), 80 µm (σ=5.0 µm) and 83 µm (σ=4.9 µm) in areas A, B, C and D respectively (Figure 2). In Tables 1-3 used dash "-" means lack of intermetallics or dendrites in the inspected area and resulting number density 0.0 mm^{-2}. The similar methodology was applied for other alloys and parameters collected in Tables 1-3.

Secondary dendrite arm spacing λ_2 changed under stirring 9% and 5%, increased from 87 µm to 95 µm and from 101 µm to 106 µm (Table 1) for the α-Al-first and α-Al-2-first alloys. Analyzing λ_2 across the specimen, when considering the standard deviation, λ_2 seems to have similar values. In the rest alloys, the distances between dendritic arms λ_2 increased as an effect of intensive flow, e.g. 57% for the Mn-2-first (AlSi12.526Mn1.365) alloy and 14% for the α-Al/Si (AlSi12.536Mn0.296) alloy. The decrease in proportion between perimeter and the area of grain S_v caused by forced convection for the α-Al-2-first (AlSi4.896Mn0.254) and α-Al-first (AlSi7.887Mn0.379) alloys amounts 40% and 42%, with stable values across sample, and similarly for the others.

The average overall dimension L_{Mn} (Feret diameter, Table 2) of inter-eutectic Mn-rich precipitates increased by 69% for the AlSi7.887Mn0.379 alloy (labeled as α-Al-first), whilst decreased (24%) for the α-Al-2-first (AlSi4.896Mn0.254) alloy. For the Mn-2-first alloy, L_{Mn} increased 31%. Under stirring, number density n_{Mn} (Table 2) decreased 47% and increased 155% for α-Al-first (AlSi7.887Mn0.379) and α-Al-2-first alloys respectively.

For pre-eutectic Mn-phases (Table 3), larger values of average overall dimension L_{Mn} (Feret diameter) was noticed, where the sizes reached 350-468 µm, in opposite to inter-eutectic precipitates 6.58-29.75 µm. Electromagnetic stirring caused smaller Mn-phases in Mn-2-first and α-Al/Mn alloys, about 20% and 24 % respectively. In both alloys, where pre-eutectic phases occurred (Table 3), number density n_{Mn} decreased. Across the cylindrical specimen (Figure 2), for Mn-2-first alloy, manganese rich phases are larger (541 µm) outside (area D, Figure 2) then inside (area A, 450 µm) for stirring, and similarly without flow, 482 µm outside and 297 µm inside. For Mn-2-first and α-Al/Mn alloys and both stirring options, number density n_{Mn} was smaller outside (area D) than inside (area A) sample.

For the spacing λ_E of the Al-Si eutectics (Table 2), stirring caused the changes in both directions, decreases and increases were observed for selected alloys, suggesting more complicated mechanism. For the Mn-2-first (AlSi12.526Mn1.365) alloy,

Table 1.
Parameters characterising α-Al phases

Aluminum Alloys	RMF [mT] {Solid. Time [s]}	Dendrites	
		λ_2 [μm]	S_v [μm^{-1}]
"α-Al-first" alloy AlSi7.887Mn0.379	0{630}	87 [5.9] (25/248) 86:104:80:83 [3.3:5.2:5.0:4.9]	0.031 [0.002] 0.032:0.030:0.033:0.029 [0.002:0.001:0.003:0.001]
	11{713}	95 [6.0] (19/128) (9%) 100:94:89:98 [4.4:6.6:8.0:5.2]	0.018 [0.001] (-42%) 0.018:0.017:0.018:0.018 [0.001:0.001:0.001:0.001]
"α-Al-2-first" alloy AlSi4.896Mn0.254	0{761}	101 [8] (28/339) 122:100:101:93 [10.4:6.3:5.7:6.2]	0.025 [0.002] 0.023:0.024:0.026:0.025 [0.001:0.002:0.003:0.002]
	11{860}	106 [15.3] (24/162) (5%) 114:100:110:102 [24.9:11.9:10.9:13.5]	0.015 [0.001] (-40%) 0.015:0.014:0.015:0.015 [0.001:0.001:0.001:0.001]
"Mn-2-first" alloy AlSi12.526Mn1.365	0{419}	51 [5.5] (23/271) 49:48:60:47 [8.4:2.7:4.2:2.1]	0.059 [0.007] 0.058:0.057:0.055:0.070 [0.003:0.006:0.008:0.008]
	11{532}	80 [10] (20/153) (57%) 93:89:91:60 [7.5:7.6:5.4:8.0]	0.027 [0.003] (-54%) 0.031:0.029:0.026:0.025 [0.002:0.003:0.003:0.002]
"α-Al/Mn" alloy AlSi7.798Mn0.835	0{827}	114 [9.0] (19/225) 142:115:114:104 [8.6:6.4:8.2:3.2]	0.028 [0.002] 0.024:0.028:0.029:0.034 [0.002:0.002:0.001:0.001]
	11{819}	127 [10.7] (18/131) (11%) 141:139:123:106 [8.8:8.4:6.3:5.2]	0.018 [0.001] (-36%) 0.018:0.016:0.019:0.018 [0.001:0.001:0.002:0.001]
"α-Al/Si" alloy AlSi12.536Mn0.296	0{530}	77 [7.6] (12/120) 78:69:89:63 [3.2:11.0:8.2:5.4]	0.032 [0.002] 0.034:0.028:0.035:0.036 [0.001:0.002:0.001:0.002]
	11{529}	88 [6.0] (9/72) (14%) 92:96:90:80 [-:8.8:6.7:4.9]	0.024 [0.003] (-25%) 0.028:0.025:0.023:0.023 [0.003:0.001:0.003:0.003]
"eutectic point" alloy AlSi12.569Mn0.579	0{540}	78 [16.0] (10/91) 104:117:105:63 [0.9:-:-:17.4]	0.029 [0.006] 0.030:0.027:0.028:0.031 [0.003:0.002:0.001:0.011]
	11{423}	76 [6.4] (15/113) (-3%) 81:74:82:72 [11.5:6.5:2.9:5.9]	0.036 [0.003] (24%) 0.040:0.043:0.034:0.032 [0.002:0.002:0.002:0.002]

(1) Dash – lack of data e.g. by absence of phases; (2) Brackets [the standard deviation]; (3) Parentheses (numbers of grains inspected/numbers of dendrite arms counted) ; (4) Curly brackets {the solidification time (s)}; (5) Parentheses (caused by forced flow variation [%] of the parameters %); (6) Parameters separated by colon : – values gained in areas A,B,C and D.

the eutectic spacing λ_E, by standard deviation values of 0.52 and 1.21 μm, increased from 4.57 to 8.95 μm (96%).

3.3. Precipitation sequence

To find the alloys compositions, that supports solidification with occurring perfectly only one phase (e.g. α-Al or Al$_{15}$Si$_2$Mn$_4$) or exactly two (e.g. α-Al and Si crystals), Thermo-Calc [20] software was applied. Calculation results (Table 4 and Figure 9) present precipitation order, characteristic temperature and for one of alloys were below described.

Based on the ternary Al-Si-Mn phase diagram (Figure 1), the alloy with composition AlSi7.8Mn0.3 was chosen, next based on many iterative calculations, with analysis of Sheil solidification and property diagrams (Figure 9a), finally the composition AlSi7.887Mn0.379 was used. In this alloy (Table 4), beginning from the temperature 610 °C, α-Al phase will start to form and the reaction will be described as L → α-Al. Because of the enrichment of the melt in Si and Mn, the concentration amounts 12.444%Si and 0.575%Mn and achieves the eutectic reaction at 576.59 °C. This reaction L → α-Al + Si starts at 576.59 °C, followed by enrichment of alloy, that reaches 12.569%Si and 0.581%Mn, finally ends with L → α-Al + Al$_{15}$Si$_2$Mn$_4$ + Si at temperature 575.88 °C. At this

stage, the mass fraction for α-Al precipitates reaches f$_{α-Al}$ = 92.66%, for Mn-rich Al$_{15}$Si$_2$Mn$_4$ phases mass fraction reaches f$_{Al15Si2Mn}$ = 0.99% and for eutectics mass fraction reaches f$_{Eut}$ = 6.35%. The precise iterative calculations presented the reaction L → α-Al + Si that was not intentional, but it occurred on only short temperature period 576.59-575.88°C. The reaction was not planed and in comparison to the range 610-576.59°C of the reaction L → α-Al, has negligible meaning. The idea of only two reactions L → α-Al and L → α-Al + Al$_{15}$Si$_2$Mn$_4$ + Si was practically fulfilled.

Similar calculations were conducted for other studied alloys (e.g. α-Al/Mn, Figure 9b) and presented in Table 4, whilst detailed descriptions was avoided to shorten this paper.

4. Discussion

The microstructure modification caused by forced convection require discussion, to note various phenomena during solidification under stirring. Here the transformation from dendritic to spheroid, the modification of amounts, dimensions and distribution of Al-Si eutectics, intermetallics, Si crystals, all captured by the measured parameters and figures, will be discussed and analyzed.

4.1. Rosettes and dendrites

In the analyzed Al-Si-Mn alloys, crystals of α-Al grew as globular grains or rosettes and dendrites (Figure 3).

Das et al. [21] showed that due to high share rate dendritic growth may be reduced in favor of globular α-Al grains. Li et al. demonstrated on water succinonitrile (SCN)-5% [22] globular growth by natural nucleation and by convection. Flemings and Martinez [23] studied intensive stirring effect on spheroidal forms in aluminum alloy. In Al-10 wt.%Cu alloy solidified by forced convection [24], the rosette-shaped forms were ripened arms of deformed α-Al phase.

The microstructure in slowly solidified alloys is characterized by specific surface S_v [25], distance between grains, grain size and secondary dendrite arm spacing $λ_2 = λ_{SDAS}$ [26–29].

Many studies [28,30–32] on the dendrites growth resulted in the simple mathematical models, where the distance between secondary arms of dendritic grains $λ_2 = λ_{SDAS}$ depends on the local solidification time t:

$$λ_2 = c_1 \cdot t^{n1} \tag{1}$$

where for the diffusive regime $n_1 = 0.33$ and 0.48 for forced flow conditions, whilst coefficient c_1 depends on the studied alloy [28, 30, 32–35].

The flow occurring from the tip to the root of secondary dendrite arm should strengthen the rate of ripening, [36]. Depending on flow conditions, the exponent should be modified n_1 from 0.33 for diffusive ripening to 0.5 as proved by Steinbach [37], Ratke and Thieringer [38] and Kasperovich [39]. For directional solidification and flow induced by electromagnetic field in strength of 6 mT, Steinbach [36] recommended n_1 equal to 0.48 instead of 0.36 in a natural convection.

Table 2.
Parameters characterizing inter-eutectic Mn phases and Al-Si eutectics

Aluminum Alloys	RMF [mT] {Solid. Time [s]}	Mn phases (inter-eutectic – small phases)		AlSi Eutectics
		L_{Mn} [μm]	n_{Mn} [mm^{-2}]	$λ_E$ [μm]
"α-Al-first" alloy AlSi7.887 Mn0.379	0{630}	7.35 [0.419] (378) 6.60:5.36:7.86:14.16 [0.201:0.139:0.412:0.683]	144.0 135.6:184.4:202.6:53.32	4.29 [0.43] 4.3:2.9:4.2:6.5
	11{713}	12.45 [0.667] (249) (69%) 10.86:10.69:14.7:15.6 [0.521:0.412:0.844:0.701]	76.81 (-47%) 83.90:97.48:107.3:18.51	5.74 [0.79] (34%) 5.3:3.1:5.9:9.7
"α-Al-2-first" alloy AlSi4.896 Mn0.254	0{761}	8.71 [0.347] (49) 5.95:10.09:7.01:11.0 [0.161:0.380:0.170:0.364]	15.12 8.64:12.34:20.98:18.51	2.89 [0.25] 2.3:1.8:3.0:4.0
	11{860}	6.58 [0.358] (124) (-24%) 4.78:5.50:7.43:8.52 [0.199:0.209:0.286:0.487]	38.25 (155%) 34.55:45.65:27.15:45.65	3.91 [0.23] (35%) 3.33:3.36:3.90:5.25
"Mn-2-first" alloy AlSi12.526 Mn1.365	0{419}	20.93 [1.498] (535) 13.27:15.70:23.17:40.50 [0.57:0.76:1.30:2.36]	203.8 129.5:316.9:263.6:105.1	4.57 [0.52] 3.2:3.8:3.7:8.2
	11{532}	27.39 [1.730] (236) (31%) 25.02:32.81:31.12:26.04 [1.30:2.48:1.94:1.54]	89.90 (-56%) 135.6:67.04:33.52:123.4	8.95 [1.21] (96%) 5.5:8.9:16.2:7.3
"α-Al/Mn" alloy AlSi7.798 Mn0.835	0{827}	20.97 [1.56] (211) 19.28:20.71:21.95:22.74 [1.20:1.21:1.87:2.08]	80.37 92.94:94.46:70.08:63.99	7.29 [0.44] 7.8:5.3:8.5:8.6
	11{819}	29.75 [3.56] (181) (42%) 20.09:49.24:42.78:22.41 [1.32:5.74:4.84:2.03]	68.94(-14%) 76.18:42.66:51.80:105.1	7.43 [0.44] (2%) 7.4:9.4:5.7:6.6
"α-Al/Si" alloy AlSi12.536 Mn0.296	0{530}	12.17 [0.922] (177) 14.71:12.27:11.72:10.50 [0.99:0.80:0.73:1.01]	67.42 73.13:30.47:73.14:92.94	15.4 [1.12] 12.1:17.8:14.4:18.9
	11{529}	10.29 [0.682] (155) (-15%) 6.74:11.73:10.96:9.11 [0.57:0.62:0.68:0.75]	59.04 (-12%) 27.42:65.51:92.94:50.28	14.39 [1.50] (-7%) 11.3:21.4:14.3:13.4
"eutectic point" alloy AlSi12.569 Mn0.579	0{540}	20.04 [1.55] (188) 15.54:22.35:15.47:27.98 [0.98:1.48:0.82:2.46]	71.61 99.03:103.6:36.56:47.23	14.92 [1.81] 10.3:12.8:17.6:21.2
	11{423}	8.41 [0.619] (592) (-58%) 7.10:6.86:11.30:9.79 [0.46:0.38:0.91:0.64]	225.5 (215%) 252.9:281.8:170.6:196.5	5.31 [0.53] (-64%) 3.8:3.7:6.7:8.0

(1) Dash – lack of data e.g. by absence of phases; (2) Brackets [the standard deviation]; (3) Parentheses (numbers of grains inspected/numbers of dendrite arms counted); (4) Curly brackets {the solidification time (s)}; (5) Parentheses (caused by forced flow variation [%] of the parameters %); (6) Parameters separated by colon : – values gained in areas A,B,C and D.

For the α-Al-first and α-Al-2-first alloys (Table 1) the induced by electric coils flow caused an 9% and 5% increase in $λ_2$, from 87 μm to 95 μm and from 101 μm to 106 μm, respectively. The standard deviation σ shows similar values for the $λ_2$ across specimen. The spacing $λ_2$ increased 57% for the Mn-2-first alloy, by 11% for the α-Al/Mn alloy, and by 14% for the α-Al/Si alloy. In the α-Al/Mn, α-Al-2-first and α-Al-first alloys, in mass fraction

dominant phase is α-Al, whilst small and negligible in e.g. α-Al/Si and other alloys (Table 4, Figure 9).

An increase in $λ_2$, based on the Equation (1) may follow from the longer solidification (Table 1), as was measured for the α-Al-first alloy solidifying by stirring. For the α-Al-first alloy processed by natural only convection, spacing amounts $λ_2 = 87$ μm, and with forced convection, calculated from (1) and solidification time

measured, the received value $\lambda_2 = 91$ μm is again smaller than the determined from microsections one $\lambda_2 = 95$ μm. To get the 95 μm spacing, coefficient n_1 in (1) should be higher (n_1=0.3365), even higher than n_1 for diffusive ripening (n_1=0.33 as by natural only convection) [37,40]. And similar results are in case of α-Al-2-first alloy, where n_1 increased very slightly from 0.330 to 0.3313, suggesting lack of flow.

Table 3.
Parameters characterizing pre-eutectic Mn intermetallics

Aluminum Alloys	RMF [mT] {Solid. Time [s]}	Mn phases (PRE-eutectic – large phases)	
		L_{Mn} [μm]	n_{Mn} [mm^{-2}]
"Mn-2-first" alloy AlSi12.526Mn1.365	0{419}	468 [32.2] (508) 450:421:459:541 [32.2:29.0:36.8:34.5]	0.896 2.51:1.29:0.85:0.53
	11{532}	375 [27.2] (219) (-20%) 297:325:345:482 [17.6:14.2:14.0:41.9]	0.386 (-57%) 0.650:0.706:0.299:0.274
"α-Al/Mn" alloy AlSi7.798Mn0.835	0{827}	459 [24.2] (522) 433:482:427:481 [22.4:26.2:22.1:25.0]	0.921 1.667:1.054:0.897:0.774
	11{819}	350 [25.3] (373) (-24%) 289:421:333:331 [20.8:31.0:23.0:23.4]	0.658 (-29%) 0.960:0.838:0.542:0.621

Table 4.
Precipitation sequence in studied AlSiMn alloys

Alloy	Reaction	Temperature Range of Reaction	Mass Fraction of Solid Phases [%] (the Rest is Liquid Alloy) at the Temperature [°C]				
			Temperature	α-Al	Al$_{15}$Si$_2$Mn$_4$	Si crystals	Al-Si Eutectics
"α-Al first" alloy AlSi7.887Mn0.379	L → α-Al	610–576.59	576.59	41.91	0	0	0
	L → α-Al + Al$_{15}$Si$_2$Mn$_4$ + Si	576.59-575.88	575.88	92.66	0.99	0	6.35
"α-Al-2 first" alloy AlSi4.896Mn0.254	L → α-Al	630–578.38	578.38	68.30	0	0	0.0
	L → α-Al + Al$_{15}$Si$_2$Mn$_4$ + Si	578.38–575.88	575.88	96.08	0.56	0	3.36
"Mn-2 first" alloy AlSi12.526Mn1.365	L → Al$_{15}$Si$_2$Mn$_4$	630–575.89	575.89	0	2.67	0	0.0
	L → α-Al + Al$_{15}$Si$_2$Mn$_4$ + Si	575.89–575.88	575.88	84.94	4.31	0	10.75
"α-Al/Mn" alloy AlSi7.798Mn0.835	L → α-Al + Al$_{15}$Si$_2$Mn$_4$	610.0–575.89	575.89	43.02	1.58	0	0.0
	L → α-Al + Al$_{15}$Si$_2$Mn$_4$ + Si	575.89-575.88	575.88	91.36	2.52	0	6.12
"α-Al/Si" alloy AlSi12.536Mn0.296 (first α-Al+Si)	L → α-Al + Si	576.44–575.89	575.89	50.72	0.0	0	6.36
	L → α-Al + Al$_{15}$Si$_2$Mn$_4$ + Si	575.89-575.88	575.88	88.18	0.72	0	11.10
"eutectic point" alloy AlSi12.569Mn0.579	L → α-Al + Al$_{15}$Si$_2$Mn$_4$ + Si	575.89-575.88	575.88	87.29	1.67	0	11.04

For the Mn-2-first alloy based on mathematical formulation (1), the solidification time measured and observed on microsections average λ_2, the corresponding equal values from calculations may be obtained when the exponent n_1 reaches higher values, instead of 0.33 for diffusion based mass transport 0.387 observed in ripening by convection, and this value is even lower than determined in experimental unidirectional solidification and proposed in [37,40]. For the eutectic point, α-Al/Mn and α-Al/Si alloys, the exponent n_1 in (1) has been changed from known and proposed in literature 0.33 to 0.339, 0.346 and 0.35 respectively. The values increased but still are smaller than the values of 0.47–0.50 found in the literature [37,40]. The values and changes observed in the coefficient n_1, may be interpreted as the signal of a lack of flow or at least weak streams of melt in presence of electromagnetic filed, if not at the beginning of solidification than at finish, the secondary arms become thicker (coarsening phenomenon). This may happen by high mass fraction of α-Al phases in α-Al/Mn, α-Al-first and α-Al-2-first alloys.

The fact that the results for λ_2 and n_1 values are lower than 0.47–0.50 [37,40], supports the concept of too small convective movement, that might form dendrites and local-only diffusive conditions. For other areas with significantly changing α-Al to rosette shaped, the flow appears not to be slowed down.

Because of the proportionality between the solidification time t and the specific interfacial area S_v, Glicksman [41] proposed:

$$S_v \sim t^{-1/3} \tag{2}$$

and S_v reached values from 0.04 to 0.22 μm^{-1} for directionally solidified Al-30 wt.%Cu alloy, for the solidification front holding time 20-500 min [42], and melt flow changed S_v from 0.077 to 0.035 μm^{-1} by 200 min.
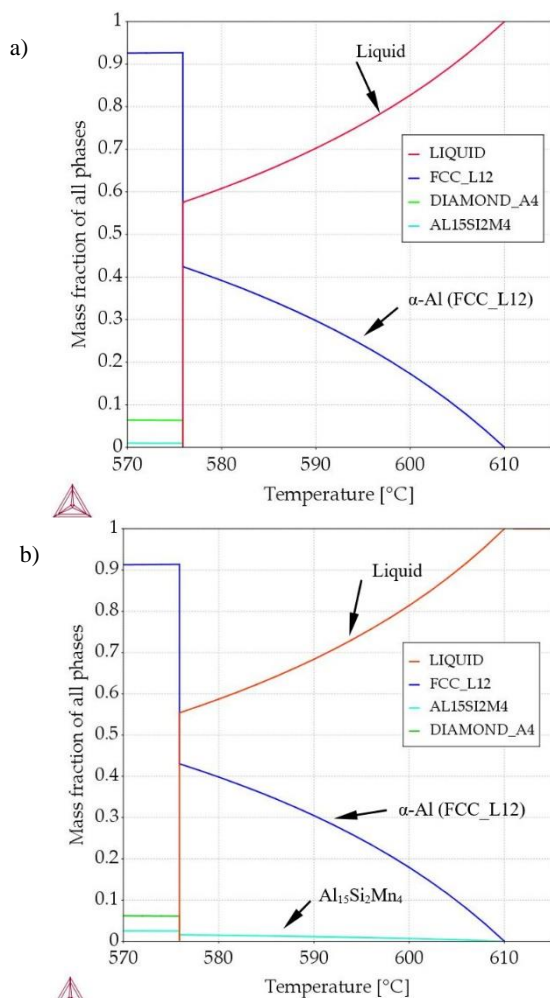
a)
b)

Fig. 9. Property diagrams for the: (a) "α-Al first" alloy and (b) the "α-Al/Mn" alloy

The 42% and 40% flow caused reduction in the specific surface S_v (Table 1) for the α-Al-first and α-Al-2-first, is significant and larger than calculated values of the standard deviation. Also across sample similar S_v reductions were observed. For the α-Al/Si alloy, S_v reduced 25%, for the α-Al/Mn alloy 36% and for the Mn-2-first alloy 54%. The proportionality (2) may be complemented by the proposed below coefficient and modified to the equation. Based on solidification time t, specific surface S_v may be estimated by application of coefficient 0.2232-0.4327 for natural only

convection and by 0.1394-0.4731 for forced convection. The specific surface S_v reacts more sensitive to the presence of movement in the melt than secondary dendrite arm spacing λ_2 and estimating flow more effectively should be used in priority.

The measured lower values of specific surface S_v show that in the microstructures occurred α-Al phases, became larger and rounder.

4.2. Eutectics

In the mechanism of eutectics formation, cooperative or without any exchange of solute between phases, growth of two (or more) phases occurs [28]. The rejected from the solid phase solutes may concentrate or flow away under melt stirring. Eutectic spacing depends on materials coefficient and the solidification front velocity [27,43], and as presented for AlSi7Mg0.6 alloy in directional solidification, spacing decreased with increased from 10 to 120 μm/s solidification velocity. As Steinbach [27] presented, also may play a role in determining spacing, where lamellar spacing increased from 4 μm without flow to 8 μm by electromagnetic field at the strength of 6 mT. The studies concerning AlSi [44] and AlSiFe alloys did not presented any influence of flow by 3 and 6 mT on eutectic spacing. Observed by Junze and Ren [45] concentration of eutectics in sample center may also influence spacing. In hypoeutectic alloys [46] solidified directionally, front solidification length reaches about 18 mm by temperature gradient 3 K/mm, and at the eutectics growth at 575 °C in 1-3 mm wide eutectic zone, the formed dendrites may dump flow and minimize its effect on eutectic spacing. At a cooling rate of 0.108 K/s and a temperature gradient of about 0.141 K/mm, in equiaxed solidification of AlMgSi [14] or AlCuSi [15] alloys, freely shaped in melt dendrites may move and seem not to stop flow, so its effect on eutectic spacing may take on meaning.

In the α-Al-first alloy occurring strong convective melt movements, increased the eutectic spacing λ_E by about 34%, from 4.29 μm to 5.74 μm (Table 2), but considering the calculated standard deviation, in this case in value of σ=0.43 and 0.79 μm, the λ_E modification seems small. In the α-Al-2-first alloy, the standard deviation amounts σ=0.25 and 0.23 μm, and λ_E increased similarly, by about 35%, from 2.89 to 3.91 μm. In the hypoeutectic alloys mass fraction amounts about 90% for α-Al and about 5% for eutectics (Table 4), and eutectics precipitate in the cavities formed by dendrites or rosettes, and by even well penetrating the sample electromagnetic field, in the cavities the movement of rest liquid may be strongly diminished. For the α-Al/Mn alloy, λ_E stayed unchanged, where probably flow was stopped by α-Al and Mn phases. In the eutectic point alloy (Table 4), by the excess of eutectics (Table 4), λ_E changed -64%, from 14.92 μm to 5.31 μm (Table 2) by σ=1.81 and 0.53 μm. When the standard deviation is ignored, we have larger changes in the eutectic spacing λ_E for alloys where the single phase grow (e.g. α-Al in α-Al-first alloy) that in alloys with joint growth of two phases (e.g. α-Al and Mn phases in α-Al/Mn alloy). Since it is only towards the end of solidification that eutectics increases massively (Table 4), when previously α-Al formed a rigid and stationary structure, forced convection seems to be only possible and reduced in the inter-dendritic cavities. The 11 mT strong field still present in the material, in the small inter-dendritic cavities, seems to generate a sufficient flow for changes

in λ_E similarly to the almost purely eutectic areas in eutectic point alloy. However, the small amount of eutectics present in the microstructure, may result in larger measurement errors in the α-Al/Mn, α-Al-first and α-Al-2-first alloys, which is in contrast to the other alloys studied.

The lack of unambiguity of results requires studies more focused on eutectic cells and stronger electromagnetic or even mechanical stirring in future experiments.

4.3. Mn-phases

The influence of forced convection on the precipitating Mn-phases in some alloys was earlier studied for AlMgSi [14] and AlCuSi [15] systems, but some similarities may be found to Fe-rich intermetallics in AlSiFe alloys.

By similar to current methodology, for AlMg5Si5Mn1 alloy [14], where Mn phases precipitate as first before α-Al and eutectics, the average overall dimension L_{Mn} of Mn-phases decreased 9% under stirring, and also in the AlCu4Si6Mn2 alloy [15] where Mn-phases precipitate as first too, L_{Mn} decreased 19%. Whilst for AlCu4Si6Mn0.65 alloy [15], Mn-phases start to precipitate about 17 ˚C after α-Al, as the second, and further joint growth occurs till solidus temperature, and flow reduced the length L_{Mn} by 42%.

For the AlSi7Mg0.2–0.6Fe0.5 alloy, the application of stirring induced by electromagnetic coils [47] resulted in the complete destruction of β-Al5FeSi phases with average length L_β of about 105 μm, and in the AlSi8Cu3Fe1.3 alloy a significant 80% reduction in the average length occurred. The average length of Fe-rich intermetallics under stirring [48] decreased in the range of L_β = 4.5–5 μm in a metal mold and in a sand mold from L_β = 9–10 μm to 7–8 μm. Inversely, in the AlSi7Fe1.0 alloy [49], the growth of large (280 μm long) β platelets in the eutectic specimen center was observed, instead of a length of 160 μm by natural only convection. Mikolajczak and Ratke [50] presented in the eutectic-rich sample center a 9% increase in the length of β platelets under flow, whilst 20% shortening in the outer dendritic microstructure. In the studied AlMgSiFeMn alloys [14], a shortening was found for equiaxed solidification, where this stirring effect was reduced in the presence of Mg2Si phases causing weaker flow. For AlCuSi system [15], average length L_β decreased 33%, from 115 to 77 μm for AlCu4Si6Fe1 alloy, whilst for AlCu10Si10Fe1 and AlCu4Si6Fe2 alloys where iron-rich phases precipitate as first, L_β increased significantly, 23 and 76 %, respectively. Histograms of Fe-phases [42] demonstrated that the increase in the number density of the small, 5-40 μm long phases, caused the reduction in L_β. In [13] was confirmed that flow by growth of β needles in the presence of α-Al phases leads to shorter Fe-phases [50], in AlSi7.837Fe0.521 L_β decreased 14%, whilst in the alloys where β precipitate as first till eutectic reaction at 575 ˚C, β-Al5FeSi grew longer, L_β increased significantly 92% in AlSi12.795Fe1.705 alloy and 76% in AlSi12.911Fe2.372 alloy. For AlSi7.508Fe1.687 alloy [13], where joint growth of β-Al5FeSi and α-Al occurred, L_β increased 17%, but earlier studies [50] suggested reduction by presence of α-Al. For AlSi15.136Fe1.678 alloy [13], where joint growth of Si crystals and β-Al5FeSi occurred, L_β decreased 22%. In both alloys, the presence of second growing phase differs significantly, there is more α-Al (higher solid fraction) in AlSi7.508Fe1.687 than Si crystals in AlSi15.136Fe1.678 alloy.

Number density n_{Mn} is the second important parameter characterizing effect of stirring on the amount of occurring intermetallics. For AlMg5Si5Mn1 alloy [14], where Mn phases precipitate as first, flow increased number density n_{Mn} 30%. For AlCu4Si6Mn0.65 alloy [15], where Mn-phases start to precipitate about 17 ˚C after α-Al, as the second after α-Al, n_{Mn} increased 53%, whilst in the AlCu4Si6Mn2 alloy where Mn-phases precipitate as first, n_{Mn} decreased 41%.

For the AlSi6.8Fe0.8 alloy [48] processed in the metal mold amount of Fe phases n_β increased only slightly under forced flow, whilst about 100% in sand mold. In directionally solidified cylindrical specimens [50] number density n_β, increased both in the eutectic center (42%) and in the dendritic outside area (17%). The addition of Mg [14] also influenced number density, and the occurrence of Mg2Si reducing flow stopped changes in n_β. In the AlCuSi system [15] by using a similar methodology, for AlCu4Si6Fe1, first α-Al precipitated and Fe-phases as the second between α-Al, the flow caused increase in number density, whilst for alloys where Fe-phases precipitated as first, AlCu10Si10Fe1 and AlCu4Si6Fe2, the number density n_β decreased, 12 and 71 %, respectively. In [13] was confirmed that flow by growth of β needles in the presence of α-Al phases leads to higher number density of Fe-phases [50], in AlSi7.837Fe0.521 n_β increased 130%, whilst in the alloys where β precipitate as first till eutectic reaction, n_β decreased significantly 71% in AlSi12.795Fe1.705 alloy and 70% in AlSi12.911Fe2.372 alloy. For AlSi7.508Fe1.687 [93], where joint growth of β-Al5FeSi and α-Al occurred, n_β decreased 26%, but earlier [50] studies suggested rise by presence of α-Al. For AlSi15.136Fe1.678 alloy [13], where joint growth of Si crystals and β-Al5FeSi occurred, L_β decreased 45%.

In the current study, the measurement of Mn-phases was divided into two groups, inter-eutectic (Table 2) and pre-eutectic (Table 3) precipitates. Inter-eutectic manganese phases have dimensions L_{Mn} in the range about 6-29 μm by number density n_{Mn} about 15-225 mm^{-2}, whilst pre-eutectic are larger L_{Mn} = 350-468 μm and less frequently occurring n_{Mn} = 0.38-0.92 mm^{-2}.

The inter-eutectic Mn phases (Table 2) precipitate at the end of solidification, and the occurring with liquidus temperature, α-Al and pre-eutectic Mn-phases should influence its growth indirectly by dumping flow, like by profusely occurring dendritical or rosette α-Al. The inter-eutectic Mn-phases in the α-Al-first alloy, become 69% larger (Table 2) under stirring, with 47% decreased number density, whilst by lower Mn content (α-Al-2-first alloy) the opposite effect was observed, smaller 24% phases by 155% increased number density were noticed. For Mn-2-first alloy, convection caused 31% (Table 2) larger Mn-phases, by 56% decreased number density. For α-Al/Mn alloy, by similar amount of α-Al phases and liquidus temperatures to α-Al-first alloy, also stirring effect was suchlike. For α-Al/Si stirring caused smaller inter-eutectic Mn-phases. Though the late precipitation of inter-eutectic Mn-phases, and its growth between other earlier formed phases, it may be pointed out some common reaction on flow in aspect of alloys composition and morphology.

The pre-eutectic Mn phases precipitate as first alone (Mn-2-first alloy, Table 3) or in common with α-Al phase (α-Al/Mn alloy). In the Mn-2-first alloy (Table 3), flow caused 20% smaller pre-eutectic phases by significantly 57% decreased number density. By the common growth of Mn and α-Al phases (α-Al/Mn alloy), stirring also caused smaller (24%) Mn precipitates together with its

29% smaller amount, and this effect occurred by plenty of grown earlier and still growing α-Al (Figure 9b). Number density across specimen has also importance, and shows different effects. Significant is the decrease in number density of Mn phases for these alloys. For Mn-2-first and α-Al/Mn alloys, across sample diameter, number density has higher values in the center than outside. Such situation seems clear according to phases diagram and real solidification front movement from crucible into center, even in such slow cooling and small gradient, where the hypoeutectic (α-Al/Mn) and eutectic (Mn-2-first) alloys solidify. Forced flow seems to keep this course of number density across sample, by generally lower values with flow. The value of the average dimension L_{Mn} of Mn phases across sample diameter has also specific distribution. For Mn-2-first, α-Al/Mn alloys, larger phases occurred outside sample (areas C and D) and flow application reduced them.

The currently observed Mn-phase shortening in Mn-2-first alloy is consistent with the results obtained in [14] for AlMg5Si5Mn1.0 alloy, where Mn-phase starts to solidify first with $T_L = 651$ ˚C till 606 ˚C, and L_{Mn} decreased 9% under stirring, in similar experimental conditions. By lower $T_L = 625$ ˚C, Mn growing first in AlCu4Si6Fe1Mn0.65 alloy [15], L_{Mn} became unchanged whilst number density decreased 56% similarly to Mn-first alloy. For α-Al/Mn similar results were observed to AlCu4Si6Mn0.65 [15], where Mn-phases started as the second at 593 ˚C after α-Al ($T_L = 610$ ˚C), the average dimension L_{Mn} decreased 42% but number density increased 53%.

4.4. Solidification by stirring

For the α-Al-first and α-Al-2-first alloys melt stirring slightly increased λ_2 by 9% and 5%, decreased S_v by 42% and 40%, and increased λ_E by 34% and 35%, respectively. Flow enlarged the inter-eutectic Mn-phases 69% in α-Al-first whilst in the α-Al-2-first alloy reduced dimension 24%. Number density n_β decreased by 47% and increased 155% respectively. The first precipitating phase α-Al, was strongly modified under stirring causing the formation of rosettes (Figure 3b) and minor dendrites, and changed the secondary spacing λ_2 as well as the specific surface, significantly. According to the ternary phase diagram (Figure 1, Table 4) the modification of Mn-phases occurs between almost fully grown dendrites (Figure 9a), causing probably some touching, breaking and deformation mechanism between the moving Mn-phases and the overwhelmingly as rosettes shaped α-Al phases.

For the Mn-2-first alloy, electromagnetic stirring increased the average overall dimension L_{Mn} of inter-eutectic Mn-phases 31% and decreased the number density n_{Mn} by 56%. For pre-eutectic large Mn-phases flow decreased L_{Mn} by 20% and decreased n_{Mn} by 57%. According to thermodynamic calculations (Figure 1, Table 4), pre-eutectic Mn-phase is the only one growing phase that independently form until solidus temperature, where eutectics precipitate. It seems, in the liquid alloy nothing can stop Mn-phases to grow large, but it precipitate in smaller amount and as smaller one by flow conditioning.

For the α-Al/Mn alloy, melt conditioning increased λ_2 by 11% from 114 μm to 127 μm, decreased S_v by 36%, decreased the L_{Mn} of pre-eutectic Mn-phases by 24%, decreased n_{Mn} by 29% and did not change λ_E. According to thermodynamic calculations (Figure 9b), α-Al and pre-eutectic phases of manganese grow together along the grove (continuous red line on Figure 1) until solidification temperature and eutectics precipitation. The decrease in L_{Mn} and n_β stays in accordance with mentioned results for Mn-2-first alloy, but precipitation sequence differs, suggesting that different growth mechanisms may occur. With the larger amount of α-Al rapidly increasing from liquidus temperature and much smaller amount of Mn-phases (Figure 9b), some mechanical interaction might be supposed. Common growth of α-Al and Mn-phases lead to formation of two kinds of Mn-phases, freely box-shaped (Figure 7b) and second one as grown in interdendritic cavities (Figure 7a).

For the α-Al/Si alloy, stirring increased λ_2 by 14%, decreased S_v by 25%, decreased the eutectic spacing by 7%, decreased average overall dimension L_{Mn} of inter-eutectic Mn-phases by 15%, decreased n_β by 12%. According to thermodynamic calculations (Figure 1, Table 4), α-Al and Si grow together along the grove (continuous green line on Figure 1) until solidification temperature and eutectics precipitation. The large dendrites observed by natural only convection (Figure 12a) disappeared (Figure 12b).

For the eutectic point alloy, electromagnetic melt stirring did not change λ_2, surprisingly increased S_v by 24%, decreased the average overall dimension L_{Mn} by 58%, increased n_{Mn} by 215% and decreased the eutectic spacing by 64%. Based on Thermo-Calc calculations (Table 4), all phases grew near solidus temperature in the eutectic reaction, meaning, in the very narrow temperature range. α-Al do not follow the pattern known from α-Al/Mn, α-Al-first and α-Al-2-first alloys, whilst inter-eutectic Mn-phases showed smaller overall dimension in growth between other precipitating phases.

Electromagnetically induced flow increased arm spacing λ_2 in the alloys, where from the liquidus temperature as first grow α-Al or start to grow from solidification beginning jointly with other phases. In almost every of the samples, α-Al phase grew with only minor dendrites and mainly as rosettes with reduced S_v. The application of flow was clearly signaled by specific surface S_v.

The current study for pre-eutectic Mn-phases in Mn-2-first alloy verified the results of [14] for bulk solidification of AlMg5Si5Mn1.0 alloy, where Mn-phases precipitated first before α-Al, and flow reduced dimension of Mn-phases by increased number density. By first growing Mn-phases but by lower liquidus temperature as in [15], for AlCu4Si6Fe1Mn0.65 the dimension was unchanged. By even lower liquidus temperature $T_L = 610$ ˚C [15] for AlCu4Si6Mn0.65 alloy, the increase in the dimension was observed. It seems that for Mn-phases and flow effect, important is precipitation temperature and precipitation sequence in relation to α-Al, in opposite to observation for iron rich β-Al₅FeSi phases [13–15,50,51].

It was observed in Mn-2-first alloy and α-Al/Mn alloy, slight tendency, to grow larger pre-eutectic Mn-phases outside specimen than in the center, by smaller number density outside than in the center, both for stirring and without it. Current study confirmed results in [13], Mn-phases change slightly location across sample diameter and do not segregate in eutectic alloy and in Mn-2-first alloy, similarly to β-Al₅FeSi phases in β-first (AlSi12.795Fe1.705) and β-2-first (AlSi12.911Fe2.372) alloys [13]. It was not observed any separation of Mn-phase, which might be similar to δ-phases separation in hypereutectic AlSi15.136Fe1.678 alloy [13].

For AlSiFe alloys [50], intensive nucleation and partial phase re-melting in unidirectionally solidified samples, was the explanation for iron-rich phases modification. The studies [13,15] proposed explanation, in that an increase in the length of iron-rich needle shaped phases follows from flow determined change in solute distribution, whilst mechanical fragmentation by interaction with α-Al or other solid phases, should lead to shortening of β-Al_5FeSi. For currently studied Mn-phases, the phenomena seems to be less connected with mechanical interaction than with precipitation temperature of phases. By high liquidus temperature, flow seems to reduce thermal and solutal diffusion layers causing reduction in constitutional undercooling, more effectively than by lower temperature and especially in the presence of other precipitated phases (e.g. α-Al dendrites or rosettes). The explanation need more detailed experiments, focused on growth mechanism of Mn-phases.

5. Conclusions

1. The induced by electromagnetic coils stirring produced mainly rosettes instead of equiaxed dendrites, reduced the specific surface S_v of α-Al, increased secondary dendrite arm spacing λ_2, changed the solidification time and AlSi eutectics,
2. Forced flow caused complex modification of inter-eutectic Mn-phases ($Al_{15}Si_2Mn_4$) depending on alloys composition and precipitation sequence.
3. In Mn-2-first alloy, where $Al_{15}Si_2Mn_4$ precipitate as first and alone, for pre-eutectic Mn-phases, forced convection decreased number density and reduced its overall dimension,
4. Stirring reduced dimension of pre-eutectic Mn-phases also by joint growth with α-Al in α-Al/Mn alloy,
5. The stirring induced movement of Mn-phases to outside area of cylindrical sample, but no separation effect was observed, as found out by iron-rich δ-phases in AlSiFe alloys,
6. The microstructure modification caused by stirring depends on the phases present, its growth sequences and temperature, and the alloys composition,
7. Current analysis on convection effect on individual precipitates in AlSiMn system, supports understanding of casting microstructure modifications occurring in technical foundry alloys with complex composition.

Acknowledgements

References

[1] Mondolfo, L.F. (1976). *Aluminium alloys: structure and properties*. Butterworths & Co.: London, UK.

[2] Glazoff, M.V., Zolotorevsky, V.S., Belov, N.A. (2007). *Casting aluminum alloys*. Elsevier Science Pub Co.: Amsterdam, The Netherlands. ISBN-10:0080453708, ISBN-13:978-0080453705. https://doi.org/10.1016/B978-0-08-045370-5.X5001-9.

[3] Mikolajczak P., Ratke L. (2014). Three dimensional morphology of mn rich intermetallics in AlSi alloys investigated with X-Ray tomography. *Materials Science Forum - Solidification and Gravity SolGrav VI.*, *Miskolc.* 790-791, 335-340. https://doi.org/10.4028/www.scientific.net/MSF.790-791.335

[4] Flemings, M. (1991). Behavior of metal alloys in the semisolid state. *Metallurgical. Transaction. B.* 22, 269-293. https://doi.org/10.1007/BF02651227.

[5] Modigell, M., Pola, A. & Tocci, M. (2018). Rheological characterization of semi-solid metals: a review. *Metals.* 8(4), 245, 1-23. https://doi.org/10.3390/met8040245.

[6] Nafisi, S., Ghomashchi, R. (2016). *Semi-Solid Processing of Aluminum Alloys*. Springer: Berlin, Germany. ISBN: 978-3-319-40333-5, DOI:10.1007/978-3-319-40335-9.

[7] Beil, W.L., Brollo, G.L. & Zoqui, E.J. (2021). A continuous casting device with electromagnetic stirring for production of ssm feedstock using Al-Si alloys. *Materials Research.* 24(3). https://doi.org/10.1590/1980-5373-MR-2020-0584.

[8] Pacheco, M.G. (2017). *Electromagnetic processing of molten light alloys reinforced by micro/nanoparticles*. Ph.D. Thesis, Universite Grenoble Alpes UGA, Grenoble, France, 13 March.

[9] Lazaro-Nebreda, J., Patel, J.B. & Fan, Z. (2021). Improved degassing efficiency and mechanical properties of A356 aluminum alloy castings by high shear melt conditioning (HSMC) technology. *Journal of Materials Processing Technology.* 294, 117146, 1-12. https://doi.org/10.1016/j.jmatprotec.2021.117146.

[10] Li, M., Murakami, Y., Matsui, I., Omura, N. & Tada, S. (2018). Imposition time dependent microstructure formation in 7150 aluminum alloy solidified by an electromagnetic stirring technique. *Materials Transactions.* 59(10), 1603-1609. https://doi.org/10.2320/matertrans.M2017357.

[11] Jin, C.K. (2018). Microstructure of semi-solid billets produced by electromagnetic stirring and behavior of primary particles during the indirect forming process. *Metals.* 8(4), 271, 1-15. https://doi.org/10.3390/met8040271.

[12] Mikolajczak, P., Janiszewski, J., Jackowski, J. (2019). Construction of the facility for aluminium alloys electromagnetic stirring during casting. In Gapiński B., Szostak M., Ivanov V. (Eds.). *Advances in manufacturing II. Vol. 4. Mechanical Engineering* (pp. 164-175). Cham, Switzerland, Springer. https://doi.org/10.1007/978-3-030-16943-5_15.

[13] Mikolajczak, P. (2023). Distribution and morphology of α-Al, Si and Fe-Rich phases in Al–Si–Fe alloys under an electromagnetic field. *Materials.* 16(9), 3304, 1-31. https://doi.org/10.3390/ma16093304.

[14] Mikolajczak, P. (2017). Microstructural evolution in AlMgSi alloys during solidification under electromagnetic stirring. *Metals.* 7(3), 89, 1-16. https://doi.org/10.3390/met7030089.

[15] Mikolajczak, P. (2021). Effect of rotating magnetic field on microstructure in AlCuSi alloys. *Metals.* 11(11), 1804, 1-23. https://doi.org/10.3390/met11111804.

[16] Mikolajczak, P., Genau, A. & Ratke, L. (2017). mushy zone morphology calculation with application of CALPHAD technique. *Metals.* 7(9), 363, 1-19. https://doi.org/10.3390/met7090363.

[17] Mikolajczak, P., Genau, A., Janiszewski, J. & Ratke, L. (2017). Thermo-Calc prediction of mushy zone in AlSiFeMn alloys. *Metals.* 7(11), 506, 1-21. https://doi.org/10.3390/met7110506.

[18] Belov, N.A., Aksenov, A.A., Eskin, D.G. (2002). *iron in aluminium alloys—impurity and alloying element.* 1st ed., Taylor and Francis Group: London, UK,. https://doi.org/10.1201/9781482265019.

[19] Shabestari, S.G. (2004). The effect of iron and manganese on the formation of intermetallic compounds in aluminum-silicon alloys. *Materials Science and Engineering: A.* 383, 289-298. https://doi.org/10.1016/j.msea.2004.06.022.

[20] Thermo-Calc 4.1—Software package from Thermo-Calc Software AB. Stockholm. Sweden. Retrieved 5 May 2023 from: www.thermocalc.se.

[21] Das, A., Ji, S. & Fan, Z. (2002). Morphological development of solidification structures under forced fluid flow: A Monte Carlo simulation. *Acta Materialia.* 50(18), 4571-4585. https://doi.org/10.1016/S1359-6454(02)00305-1.

[22] Li, T., Lin, X. & Huang, W. (2006). Morphological evolution during solidification under stirring. *Acta Materialia.* 54(18), 4815-4824. https://doi.org/10.1016/j.actamat.2006.06.013.

[23] Martinez. R.A. & Flemings, M.C. (2005). Evolution of particle morphology in semisolid processing. *Metallurgical and Materials Transactins A.* 36, 2205-2210. https://doi.org/10.1007/s11661-005-0339-1.

[24] Niroumand, B. & Xia, K. (2000). 3D study of the structure of primary crystals in a rheocast Al-Cu alloy. *Materials Science and Engineering: A.* 283(1-2), 70-75.

[25] Mendoza, R., Alkemper, J., Voorhees, P. (2003). The morphological evolution of dendritic microstructures during coarsening. *Metallurgical and Materials Transactions A.* 34, 481-489. https://doi.org/10.1007/s11661-003-0084-2.

[26] Kurz, W.D. Fisher, (1992). *Fundamentals of Solidification.* Trans Tech Public: Bäch, Switzerland, 85-90.

[27] Dantzig, J.A., Rappaz, M. (2009). *Solidification.* EPFL Press: Lausanne, Switzerland. ISBN 9780849382383.

[28] Stefanescu, D. (2009). *Science and Engineering of Casting and Solidification.* Springer: Boston, MA, USA. ISBN 978-0-387-74609-8. https://doi.org/10.1007/b135947.

[29] Wang, C.Y. & Beckermann, C. (1996). Equiaxed dendritic solidification with convection: Part II. numerical simulations for an Al-4 Wt Pct Cu Alloy. *Metallurgical and Materials Transactions A.* 27A, 2765-2783. https://doi.org/10.1007/BF02652370.

[30] Kattamis, T.Z., Flemings, M.C. (1965). Dendrite morphology. Microsegregation and Homogenization of low alloy steel. *Transactions of the Metallurgical Society of AIME.* 233(5), 992-999.

[31] Rappaz, M. & Boettinger, W. (1999). On dendritic solidification of multicomponent alloys with unequal liquid diffusion coefficients. *Acta Materialia.* 47(11), 3205-3219. https://doi.org/10.1016/S1359-6454(99)00188-3.

[32] Bouchard, D. & Kirkaldy, J.S. (1997). Prediction of dendrite arm spacing in unsteady- and steady-state heat flow. *Metallurgical and Materials Transactions B.* 28, 651-663.https://doi.org/10.1007/s11663-997-0039-x.

[33] Mortensen, A. (1991). On the rate of dendrite arm coarsening. *Metallurgical Transactions A.* 22, 569-574. https://doi.org/10.1007/BF02656824.

[34] Voorhees, P.W. & Glicksman, M.E. (1984). Ostwald ripening during liquid phase sintering—Effect of volume fraction on coarsening kinetics. *Metallurgical Transactions A.* 15, 1081-1088. https://doi.org/10.1007/BF02644701.

[35] Ferreira, A.F., Castro, J.A., Ferreira, L.O. (2017). Predicting secondary-dendrite arm spacing of the Al-4.5wt%Cu alloy during unidirectional solidification. *Materials Research.* 20(1), 68-75. https://doi.org/10.1590/1980-5373-MR-2015-0150.

[36] Mullis, A.M. (2003). The effects of fluid flow on the secondary arm coarsening during dendritic solidification. *Journal of Materials Science.* 38, 2517-2523. https://doi.org/10.1023/A:1023977723475.

[37] Steinbach, S. & Ratke, L. (2007). The influence of fluid flow on the microstructure of directionally solidified AlSi-base alloys. *Metallurgical and Materials Transactions A.* 38, 1388-1394. https://doi.org/10.1007/s11661-007-9162-1.

[38] Ratke, L. & Thieringer, W.K. (1985). The influence of particle motion on ostwald ripening in liquids. *Acta Matallurgica.* 33, 1793-1802. https://doi.org/10.1016/0001-6160(85)90003-3.

[39] Kasperovich, G., Genau, A., Ratke, L. (2011). Mushy zone coarsening in an AlCu30 alloy accelerated by a rotating magnetic field. *Metallurgical and Materials Transactions A.* 42, 1657-1666. https://doi.org/10.1007/s11661-010-0542-6.

[40] Diepers, H.J., Beckerman, C. & Steinbach, I. (1999). Simulation of convection and ripening in a binary alloy mush using the phase field method. *Acta Materialia.* 47(13), 3663-3678. https://doi.org/10.1016/S1359-6454(99)00239-6.

[41] Marsh, S.P. & Glicksman, M.E. (1996). Overview of geometric effects on coarsening of mushy zones. *Metallurgical and Materials Transactions A.* 27, 557-567. https://doi.org/10.1007/BF02648946.

[42] Loué, W.R. & Suéry, M. (1995). Microstructural evolution during partial remelting of AlSi7Mg alloys. *Materials Science and Engineering: A.* 203(1-2), 1-13. https://doi.org/10.1016/0921-5093(95)09861-5.

[43] Jackson, K.A. & Hunt, J.D. (1966). Lamellar and rod eutectic growth. *Transactions of the Metallurgical Society of AIME.* 236, 1129-1142.

[44] Sous, S. (2000). *Instationäre Erstarrung Eutektischer Al-Si Legierungen.* Ph.D. Thesis, RWTH, Aachen, Germany,.

[45] Ren Z. & Junze J. (1992). Formation of a separated eutectic in Al-Si eutectic alloy. *Journal of Materials Science.* 27, 4663-4666. https://doi.org/10.1007/BF01166003.

[46] Mikolajczak, P. & Ratke, L. (2015). Thermodynamic assessment of mushy zone in directional solidification. *Archives of foundry Engineering.* 15(4), 101-109. DOI: 10.1515/afe-2015-0088.

[47] Fang, X., Shao, G., Liu, Y.Q. & Fan, Z. (2007). Effects of intensive forced melt convection on the mechanical properties of Fe containing Al-Si based alloys. *Material Science and Engineering: A.* 445-446, 65-72. https://doi.org/10.1016/j.msea.2006.09.038.

[48] Nafisi, S., Emad, D., Shehata, T. & Ghomashchi, R. (2006). Effects of electromagnetic stirring and superheat on the microstructural characteristics of Al-Si-Fe alloy. *Materials Science and Engineering* A. 432(1-2), 71-83. https://doi.org/10.1016/j.msea.2006.05.076.

[49] Steinbach, S., Euskirchen, N., Witusiewicz, V., Sturz, L. & Ratke, L. (2007). Fluid flow effects on intermetallic phases in Al-cast alloys. *Transactions of Indian Institute of Metals.* 60(2), 137-141.

[50] Mikolajczak, P. & Ratke, L. (2013). Effect of stirring induced by rotating magnetic field on β-Al$_5$FeSi intermetallic phases during directional solidification in AlSi alloys. *International Journal of Cast Metals Research.* 26, 339-353. https://doi.org/10.1179/1743133613Y.0000000069.

[51] Mikolajczak, P. & Ratke, L. (2011). Intermetallic phases and microstructure in AlSi alloys influenced by fluid flow. Supplemental Proceedings: General Paper Selections. 3, 825-832.. DOI:10.1002/9781118062173.ch104 .